IJMMM International Journal of Minerals, Metallurgy and Materials 矿物冶金与材料学报（英文版）

A comparative study between friction stir processing and friction stir vibration processing to develop magnesium surface nanocomposites

Behrouz Bagheri, Mahmoud Abbasi, Amin Abdollahzadeh, and Amir Hossein Kokabi

Cite this article as:
Behrouz Bagheri, Mahmoud Abbasi, Amin Abdollahzadeh, and Amir Hossein Kokabi, A comparative study between friction stir processing and friction stir vibration processing to develop magnesium surface nanocomposites, *Int. J. Miner. Metall. Mater.*, 27(2020), No. 8, pp. 1133-1146. https://doi.org/10.1007/s12613-020-1993-4

View the article online at SpringerLink or IJMMM Webpage.

International Journal of Minerals, Metallurgy and Materials
Volume 27, Number 8, August 2020, Page 1133
https://doi.org/10.1007/s12613-020-1993-4

A comparative study between friction stir processing and friction stir vibration processing to develop magnesium surface nanocomposites

Behrouz Bagheri[1)], *Mahmoud Abbasi*[2)], *Amin Abdollahzadeh*[3,4)], *and Amir Hossein Kokabi*[3)]

1) Department of Mining and Metallurgy, Amirkabir University of Technology, Tehran, Iran
2) Faculty of Engineering, University of Kashan, Ravandi Blvd., Kashan, Iran
3) Department of Materials Science and Engineering, Sharif University of Technology, Tehran, Iran
4) Institute of Materials Engineering and Advanced Processes, Department of Mining and Metallurgy, Amirkabir University of Technology, Tehran, Iran
(Received: 6 October 2019; revised: 31 January 2020; accepted: 1 February 2020)

Abstract: Friction stir processing (FSP) can be used to improve surface composites. In this study, a modified method of FSP called friction stir vibration processing (FSVP) was applied to develop a surface composite on AZ91 magnesium alloy. In this technique, the workpiece is vibrated normal to the processing direction. The results illustrated that compared with the FSP method, the FSVP caused a better homogeneous distribution of SiC particles in the microstructure. The results also showed that matrix grains of friction stir vibration processed (FSV-processed) samples ((26.43 ± 2.00) μm) were finer than those of friction stir processed (FS-processed) specimens ((39.43 ± 2.00) μm). The results indicated that the ultimate tensile strength (UTS) of FSV-processed specimens (361.82 MPa) was higher than that of FS-processed specimens (324.97 MPa). The higher plastic strain in the material during FSVP, due to workpiece vibration, resulted in higher dynamic recrystallization, and consequently, finer grains were developed. The elongation and formability index of the FSV-processed specimen (16.88% and 6107.52 MPa·%, respectively) were higher than those of the FS-processed sample (15.24% and 4952.54 MPa·%, respectively). Moreover, the effects of FSVP were also found to intensify as the vibration frequency increased.

Keywords: friction stir processing; friction stir vibration processing; surface composite; mechanical properties; microstructure

1. Introduction

Magnesium alloys, because of their high strength-to-mass ratio as well as high stiffness, have gained recognition in the production of lightweight materials [1–2]. Because of their hexagonal close-packed crystallographic structure, they display moderate strength, low ductility, and low hardness at ambient temperature [3–6]. Many of these restrictions can be eliminated using effective deformation methods such as equal channel angular extrusion [7], high-pressure torsion [8], and accumulated roll bonding [9]. However, these methods are bulk deformation processes, and they affect all regions of the material. Friction stir processing (FSP) is a technique that affects only the surface of the material and improves the microstructure and mechanical characteristics of the material.

In FSP, a non-consumable tool including of a shoulder and pin is forced into the workpiece until the bottom surface of the shoulder is in touch with the workpiece surface and the pin is plunged in the workpiece. The severe contact between the tool and the workpiece produces high heat and softens the material around the welding tool. The tool is stirred as it is pushed laterally through the workpiece. Intense and localized plastic deformation of material occurs around the tool, and the properties of the metal change [10]. Friction stir processing can also be used to incorporate the strengthening particles in the metal matrix and develop metal matrix composites. Asadi *et al.* [11] applied FSP to fabricate ultrafine-grained AZ91 composite layers with nano-sized SiC particles. They reported that these reinforcing particles led to an increase in mechanical properties such as hardness. Arora *et al.* [12] used two kinds of reinforcing particles, TiC and Al_2O_3, for the FSP of AZ91 magnesium alloy and found that the microstructure and mechanical characteristics improved for AZ91/(TiC + Al_2O_3) composite. Ahmadkhaniha *et al.* [13] investigated the fabrication of the AZ91/Al_2O_3 composite layer by FSP. Their results indicated that nano-sized reinforcements have a great effect on the enhancement of the

Corresponding author: Behrouz Bagheri E-mail: b.bagheri@aut.ac.ir

magnesium alloy hardness.

The non-homogeneous distribution of strengthening particles should be avoided. Different methods such as the application of multiple processing passes and various traverse and rotational speeds are used to develop the distribution homogeneity of second-phase particles in the metal matrix. Feng *et al.* [14] used the multi-pass technique during the FSP of Mg–Al–Zn cast alloy. They discovered that the multi-pass method produced a nanocomposite layer with high mechanical properties and a sound microstructure. Asadi *et al.* [15] examined the importance of rotational and traverse speeds on the microstructure and hardness of a friction stir processed (FS-processed) layer with and without particles in the Mg matrix. They indicated that the influence of rotational and traverse speeds was negligible when nano-sized particles were incorporated in the microstructure and their effect was significant when nano-sized particles were not in the microstructure. Abbasi *et al.* [16] analyzed the microstructure, corrosion, and mechanical characteristics of FS-processed AZ91 alloy with the addition of SiC and Al_2O_3 particles to the alloy surface. The results illustrated that the strength (mechanical property), wear, and the corrosion behavior of FS-processed specimens improved significantly. The importance of the FSP pass number on the mechanical characteristics and microstructure of AZ91 alloys during FSP was examined by Dadaei *et al.* [17]. They found that mechanical characteristics namely hardness, strength, and microstructure were enhanced with an increase in the pass number. Eftekharinia *et al.* [18] analyzed the effects of pin geometry on different characteristics of 6061-T6 aluminum alloy surface composites fabricated via FSP and incorporated with SiC particles. They discovered that pin geometry played a dominant role in the distribution of SiC particles in the stir zone.

Kumar [19] designed a setup for using ultrasonic waves to apply vibration to the tool during FSP. This method was called ultrasonic-assisted friction stir processing (UaFSP). He analyzed the impacts of UaFSP on the microstructure and mechanical characteristics of processed specimens and found that the ultrasonic vibration generated high heat in the stir zone, caused intense plastic deformation, and improved the material flow. Higher ultimate tensile strength (UTS) and hardness were observed for the UaFS-processed specimen compared with those of the FS-processed specimens. Baradarani *et al*. [20] examined the influence of UaFSP on the microstructure, corrosion performance, and mechanical characteristics of AZ91 magnesium alloys. It was found that the corrosion current density of UaFS-processed specimens was about 2.09 μA/cm^2, while that of FS-processed specimens was about 3.42 μA/cm^2. The authors found that UaFSP altered the morphology and distribution of the β-$Mg_{17}Al_{12}$ phase and led to a better distribution of this phase compared with FSP. Farshbaf Zinati [21] applied the UaFSP to disperse multi-walled carbon nanotubes (MWCNTs) in a nylon 6 matrix. He found that the MWCNTs were homogeneously dispersed throughout the matrix and the micro-hardness increased as UaFSP was applied.

Based on the idea behind the UaFSP, in which the welding tool is vibrated by ultrasonic waves, in the current research, a machine was designed to vibrate the workpiece during the FSP. The workpiece is vibrated through the camshaft mechanism. In this investigation, the workpiece is vibrated during the FSP operation. This technique is called friction stir vibration processing (FSVP). The impacts of the tool traverse speed and workpiece vibration frequency on the mechanical and microstructural features of AZ91/SiC surface composite were investigated.

2. Experimental

This investigation was carried out using an AZ91 magnesium alloy sheet with a thickness of 3 mm and chemical composition (wt%) of Al 9.1, Zn 0.68, Mn 0.21, Si 0.085, Fe 0.0029, Cu 0.0097, Ni 0.001, and Mg (base element). The microstructure of the as-received metal featured a β-$Mg_{17}Al_{12}$ phase with a network-like morphology fundamentally distributed at the grain boundaries [22].

Rectangular samples with a dimension of 100 mm × 200 mm were prepared from the as-received plate. FSP was carried out along the length dimension. FSP and FSVP were performed by a milling machine. For FSP, the specimen was fixed on the fixture, and the fixture was placed on the milling machine, while for FSVP, the specimen was fixed on a vibrating machine installed on the milling machine. The camshaft mechanism was applied to transform the rotational movement of the motor shaft to the linear and reciprocating movement of the vibrating machine. The view design of the machine applied for FSVP is shown in Fig. 1. The vibration amplitude was 0.5 mm, and the specimen was vibrated in a direction normal to the processing line. The rotational speed of the motor shaft was adjusted by a driver, and the vibration frequency was consequently adjusted. To determine the influence of the improved joining method on the microstructure and mechanical characteristics, various welding conditions were utilized.

Vibration frequencies of 20, 35, and 50 Hz were applied in the current research, and different traverse speeds of 40, 63, and 95 mm/min were also applied. For all FSP and FSVP experiments, the rotational speed of the tool was 1250 r/min. These values were selected based on a trial and error method. Our studies indicated that the vibration frequency value does not have an effect on the formation of any defect and only improves the characteristics of the joints. However, for frequency values higher than 50 Hz, the changes are insignificant.

The welding tool, including shoulder and pin, was made of M2 steel. The view design of the welding tool utilized for

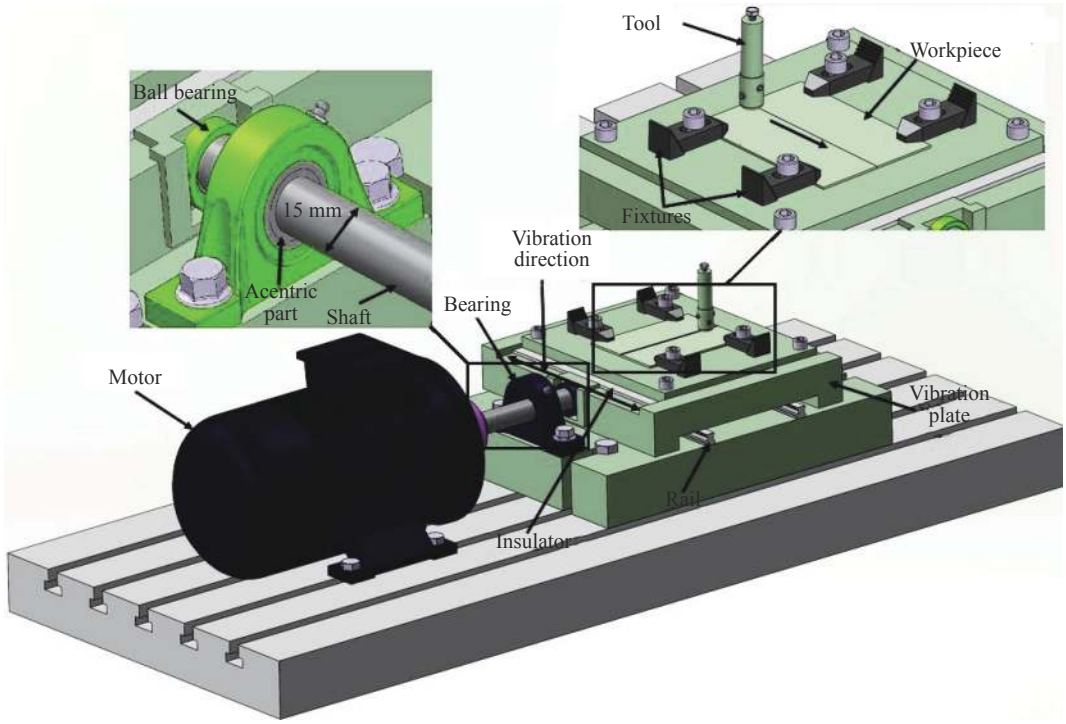

Fig. 1. Schematic of the machine used for FSVP.

FSP and FSVP is shown in Fig. 2. Moreover, SiC powder particles with a size of 50 nm were used as strengthening particles. For all the specimens, the same mass of powders (0.07 g) was applied. Initially, a V-shape groove was cut on the surface of each specimen. The groove was filled with particles. A pin-less tool was used to rub the surface and to encapsulate the particles in the specimen. Finally, FSP or FSVP was performed on the specimen. For all the experiments, the tilt angle was 2°.

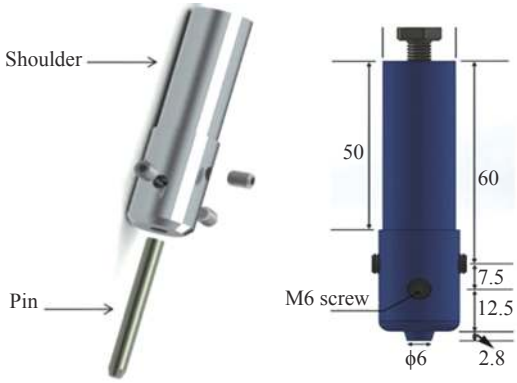

Fig. 2. Schematic of the tool utilized for FSP and FSVP (mm).

Metallography techniques were applied to reveal the microstructure and SiC particle distribution in the samples. The samples were etched by a solution of acetic acid (5 mL), nitric acid (7 mL), water (10 mL), picric acid (6 g), HCL (5 mL), and ethanol (100 mL) for 3–5 s. A scanning electron microscope as well as optical microscopes were applied to observe the nano-sized SiC particle distribution, material flow, and microstructure. The method of mean linear intercept according to the ASTM-E112 standard test [23] was employed to analyze the grain size. To determine the grain size, a rectangle of the selected area was overlaid on a micrograph, and the grains in the field area were counted. The count was the sum of the number of the grains completely within the area in addition to one half of the number of grains intersected through the circumference of the area. Assuming that the grains are equiaxed and spherical in shape, the number of grains per unit area was measured, and the average diameter of grains was determined.

A uniaxial tensile test according to the ASTM-E8 standard test method [24] was used to determine the mechanical characteristics of the processed samples. Mini tensile test samples were prepared from processed samples using electro-discharge machining (wire cut). The gauge length was normal to the processing line, and the stir zone was in the middle of the gauge length. Tensile tests were done by an Instron machine with a crosshead speed of 0.5 mm/min. Vickers hardness technique was utilized to measure the microhardness of different specimens. A programmable hardness test machine was applied, and the load and dwell time for the hardness testing were 1 N and 10 s, respectively.

3. Results and discussion

Fig. 3 displays the stir zone microstructures of the FS-processed specimens at traverse speeds of 40, 63, and 95

mm/min with a rotational speed of 1250 r/min. The grain size reduced as the traverse speed increased: (53.23 ± 2.00) μm for 40 mm/min, (39.43 ± 2.00) μm for 63 mm/min, and (30.71 ± 2.00) μm for 95 mm/min. The main reason is attributed to the impact of the heat generation during FSP on the grain size. Severe contact between the tool shoulder and the surface specimen results in high heat and increases the temperature [25]. Heat transfer to the specimen decreases, and consequently, the specimen temperature increases slightly as the tool traverse speed increases. There is a direct relationship between the temperature and grain size, as the grain size increases with temperature [26]. As a result, by increasing the tool traverse speed finer grains were improved in the stir zone.

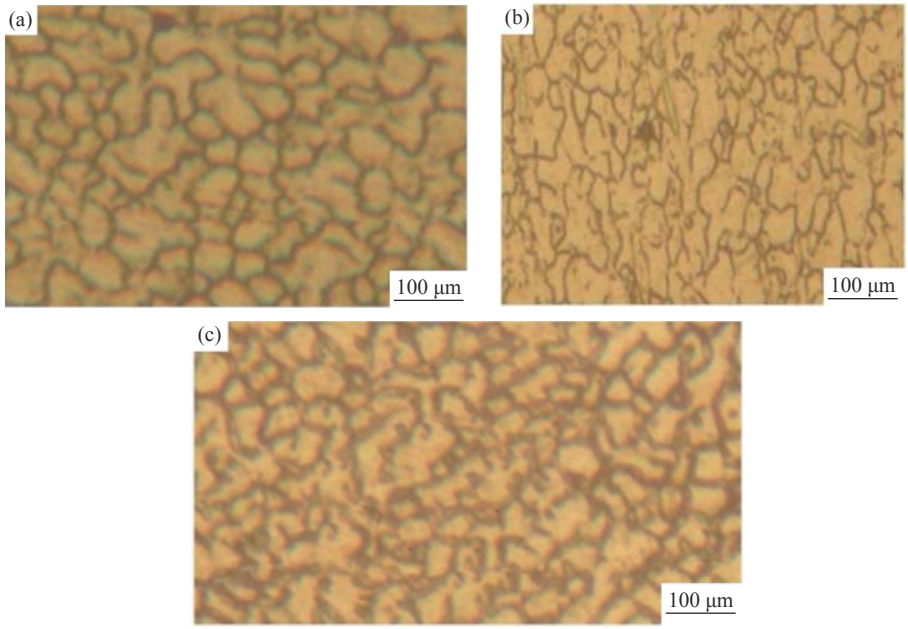

Fig. 3. Stir zone microstructures of FS-processed samples subjected to a rotational speed of 1250 r/min and different traverse speeds: (a) 40 mm/min; (b) 63 mm/min; (c) 95 mm/min.

Stir zone microstructures of friction stir vibration processed (FSV-processed) specimens subjected to various vibration frequencies are depicted in Fig. 4. For these samples, the rotational and traverse speeds are the same. Comparing the microstructure presented in Fig. 3 with those presented in Fig. 4 depicts that the FSV-processed samples had finer grains compared with the FS-processed specimens. On the other side, Fig. 4 shows that the grain size decreased as the vibration frequency increased: (33.32 ± 2.00) μm for 25 Hz, (26.43 ± 2.00) μm for 35 Hz, and (20.02 ± 2.00) μm for 50 Hz.

These observations can be associated with the effect of specimen vibration in FSVP. Specimen vibration, as well as the traverse and stir motions of the tool, leads to higher deformation of the material during FSVP compared with that during FSP [27]. Hull and Bacon [28] found that dislocation density increases as strain and material deformation increase. High temperature, because of the contact between the welding tool and specimen, and the presence of dislocations results in the possibility of dynamic recrystallization (DR) [29]. Dynamic recrystallization is the fundamental mechanism with respect to grain refinement during FSP [29–30]. Higher deformation and strain of material in FSVP lead to more intensified DR, and finer grains are consequently developed.

This can also be validated based on the relationship presented by Chang *et al*. [31]. They found that the strain rate ($\dot{\epsilon}$) during FSP can be represented based on Eq. (1):

$$\dot{\epsilon} = \frac{R_p 2\pi r_e}{L_e} \tag{1}$$

where R_p is the pin rotational speed, and r_e and L_e are the effective radius and depth of the dynamically recrystallized zone, respectively [32].

Due to specimen vibration, the r_e in FSVP is higher than that in FSP (Fig. 5). Therefore, the strain rate in FSVP is higher than that in FSP. The Zener–Hollomon parameter (Z) is dependent on strain rate [32],

$$Z = \dot{\epsilon} \exp\left(\frac{Q}{RT}\right) \tag{2}$$

where Q is the activation energy, R is the gas constant, and T is the temperature. There is an inverse relationship (Eq. (3)) between Z and the grain size (d) [33]: the grain size reduces as the strain rate increases:

$$d^{-1} = a\ln Z - b \tag{3}$$

where a and b are constants. Therefore, the grains of FSV-processed samples are predicted to be smaller than those of

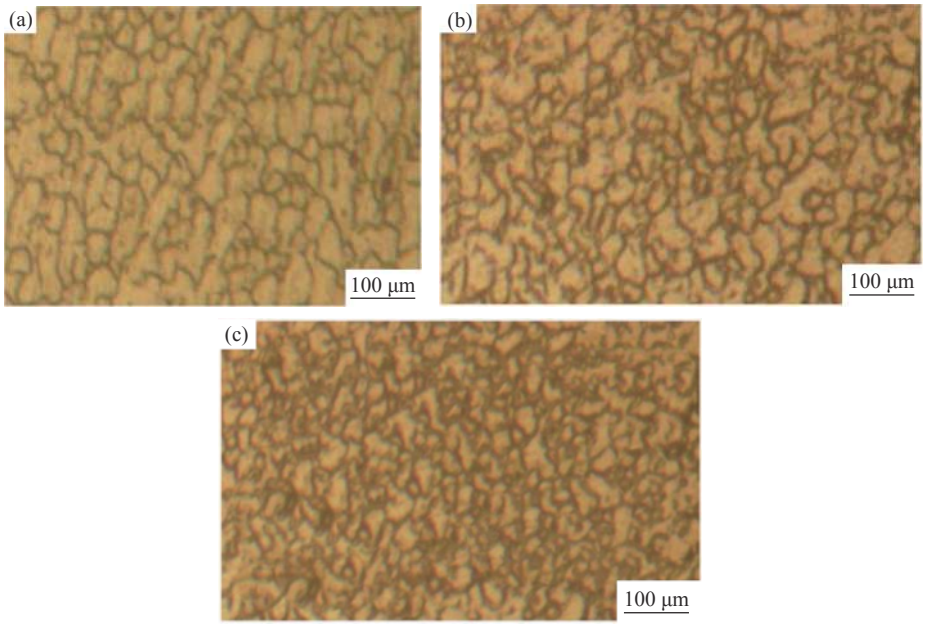

Fig. 4. Stir zone microstructures of FSV-processed samples subjected to a rotational speed of 1250 r/min, traverse speed of 63 mm/min, and different vibration frequencies: (a) 20 Hz; (b) 35 Hz; (c) 50 Hz.

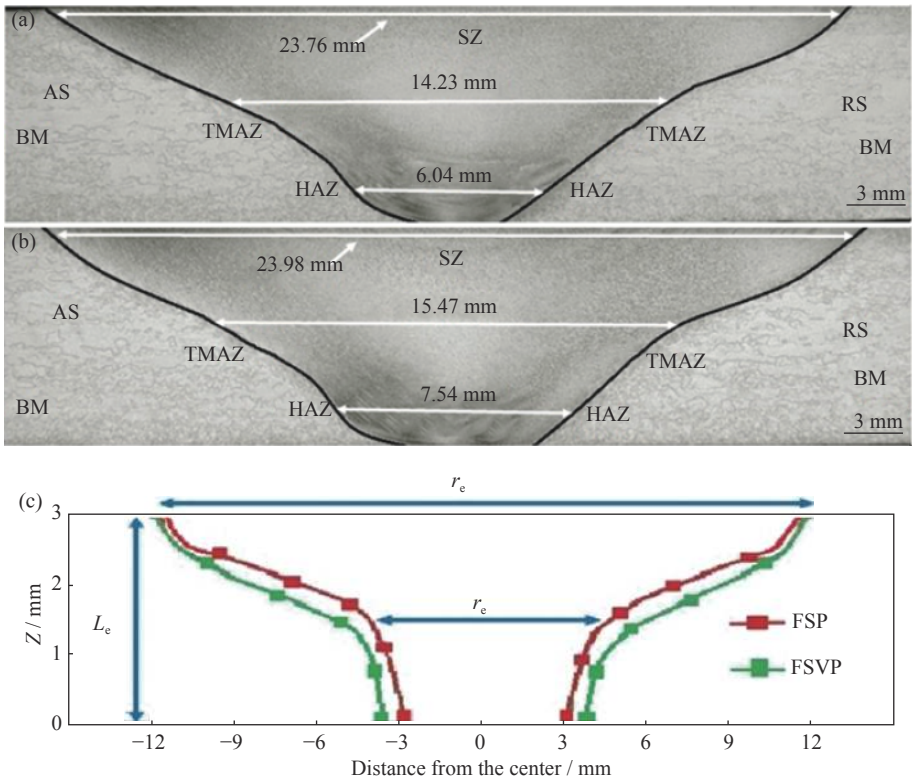

Fig. 5. Macrographs of stir zone for (a) FSP and (b) FSVP and (c) comparison of material flow in the processed zone for FSP and FSVP. AS—Advanced side; BM—Base metal; TMAZ—Thermomechanical affected zone; HAZ—Heat-affected zone; SZ—Stir zone; RS—Retreating side.

FS-processed samples. During FSVP, the material deformation, strain rate, and strain also increase as the vibration frequency increases. The higher amount of dislocation density results in a more extensive DR, and consequently, finer grains are developed.

Fig. 6 compares the light optical microscopy (LOM) images of the microstructures of FS- and FSV-processed specimens containing SiC particles. Due to the vibration, the dis-

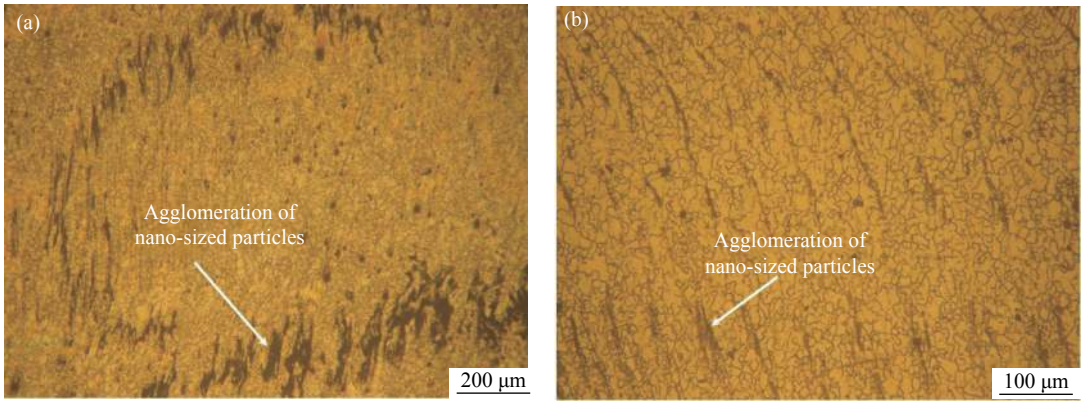

Fig. 6. LOM microstructure images of (a) FS-processed sample and (b) FSV-processed sample.

tribution of nano-sized SiC particles in the FSV-processed samples was more homogeneous in comparison to specimens produced by friction stir process.

Fig. 7 presents the scanning electron microscopy (SEM) images of nano-sized SiC particle distribution in FS- and FSV-processed samples and the energy-dispersive X-ray (EDX) spectroscopy analysis results. Particle agglomeration in the FSV-processed samples was less than that in the FS-processed samples, and the particle distribution homogeneity increased with the application of FSVP. The authors believe that the agglomerated particles break up as vibration is applied, and thus, the refining particles become more homogeneously distributed. This outcome agrees well with the results from Ref. [34]. Abbasi *et al*. [34] reported that the uniformity of particle distribution in an AZ91 alloy matrix was enhanced as the pass number increased, due to the breaking up of the agglomerated particles. Furthermore, Zener pining effect can be considered as another reason for a more homogeneous distribution of particles in the matrix. According to this effect, second-phase particles hinder grain growth by pinning the grain boundaries [35]. Therefore, intensified dynamic recovery and recrystallization as well as Zener pining are considered the significant reasons for the finer grains of the FSV-processed samples compared with those of the FS-processed samples.

The SEM images of agglomerated particles in FS-pro-

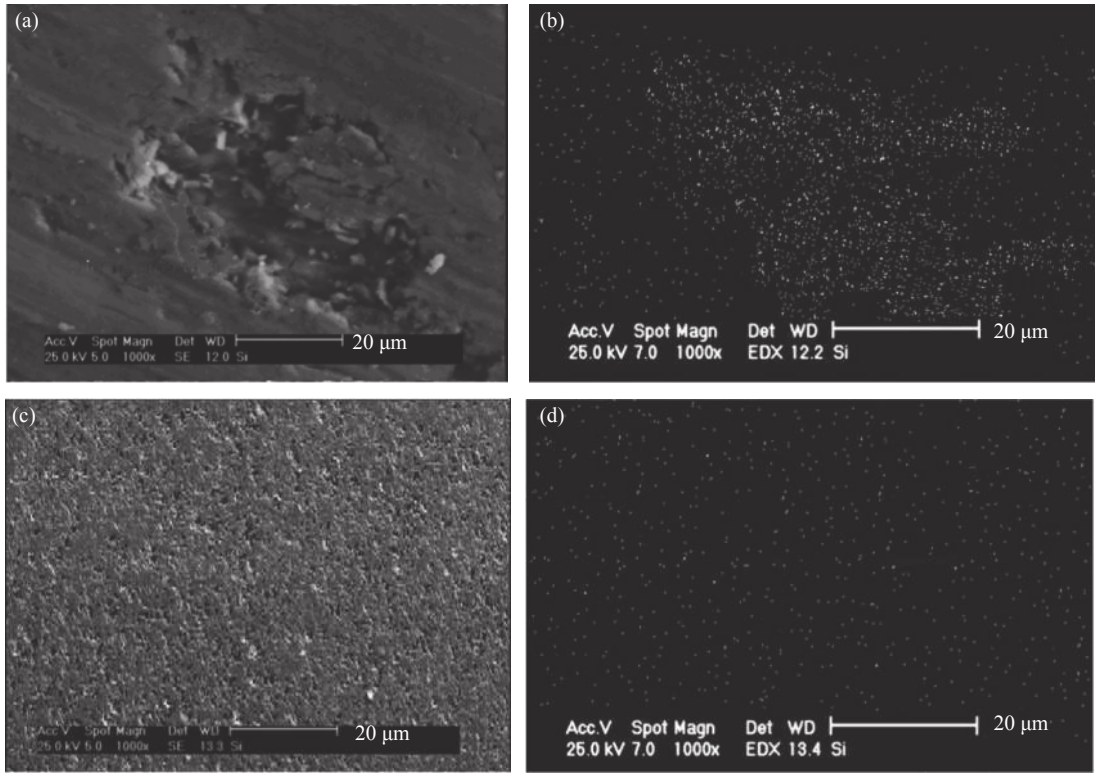

Fig. 7. (a, c) SEM images and (b, d) EDX analyses to compare the nano-sized SiC particle distribution for (a, b) FSP and (c, d) FSVP.

cessed samples containing SiC particles and processed with various traverse speeds are shown in Figs. 8(a), 8(c), and 8(e). The EDX analysis results of these specimens are also presented in Figs. 8(b), 8(d), and 8(f). High-intensity Si peaks can be observed for these particles. Fig. 8 shows that particle agglomeration decreased as the traverse speed increased. As previously mentioned, heat is generated during FSP and FSVP due to the contact between the welding tool and metal surface [36]. The heat is transferred to the metal matrix, and it softens the material around the welding tool. So, the material is deformed severely as tool moves and second-phase particles are distributed in the matrix. As the tool traverse speed decreases, heat transfer to the material around the welding tool increases, and temperature increases. At high temperature values, SiC particles have higher tendency to attach to each other and agglomeration is higher [37].

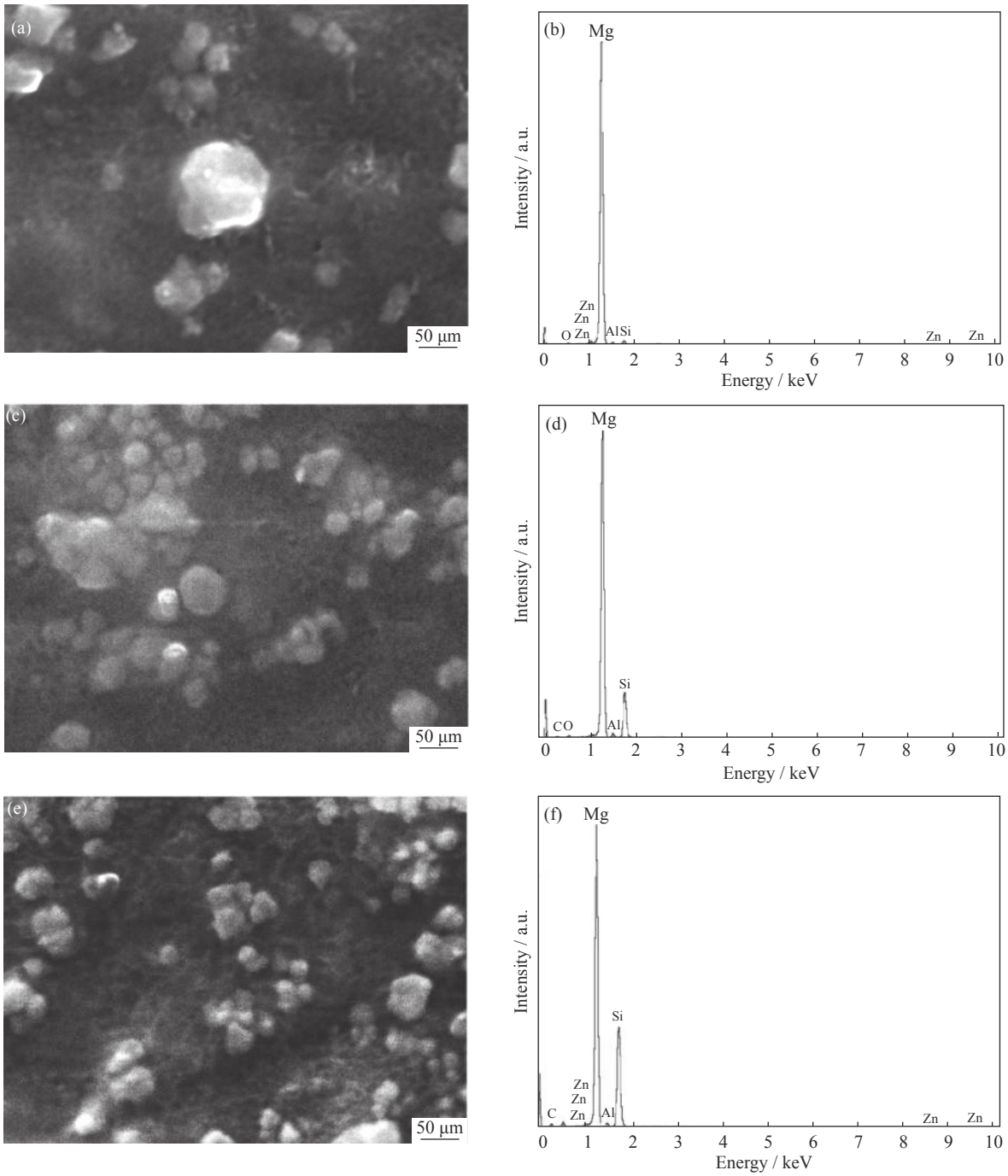

Fig. 8. (a, c, e) SEM micrographs and (b, d, f) EDX analyses of FS-processed samples subjected to a rotational speed of 1250 r/min and various traverse speeds: (a, b) 40 mm/min; (c, d) 63 mm/min; (e, f) 95 mm/min.

However, it should be noted that at very large values of transverse speed which temperature in the stir zone is very low, material deformation in the stir zone decreases and SiC agglomeration is high [22].

The transmission electron microscopy (TEM) analysis results of FS- and FSV-processed samples with no SiC particles are shown in Fig. 9. Both specimens were processed using the same rotational and traverse speeds. Fig. 9 presents the β-particle distribution within the microstructure. The β-phase was not continuous, and it was transformed into separate particles. According to Fig. 9, the β particles of FS-processed samples were larger than those of FSV-processed samples. Gajanan *et al*. [38] found that the β particles of as-received AZ91 magnesium alloy dissolved as heat production increased. Fig. 9(b) shows that some β particles were on the grain boundaries (red arrows), while some were not (yellow arrows). Moreover, β-phase particles may also reduce the mobility of dislocations and improve the strength; however, Baradarani *et al*. [20] found that their detrimental effect on crack formation is higher than their advantageous role.

The LOM images of the stir zones of FSV-processed samples containing SiC particles and processed by various vibration frequencies are displayed in Fig. 10. The homogeneity distribution of second-phase particles was improved, and the size of agglomerated particles decreased as the vibration frequency improved. As the vibration frequency improved, the motion of material in the stir zone increased, and consequently, the particle distribution homogeneity increased.

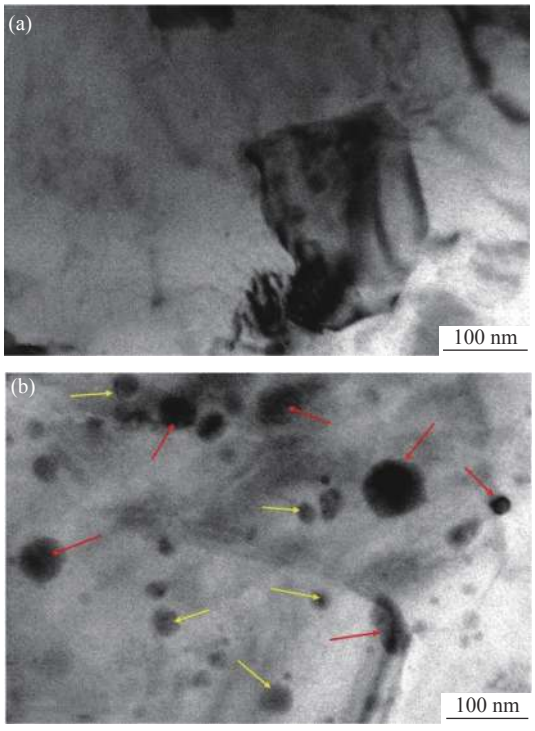

Fig. 9. TEM images of the processed samples: (a) FSP; (b) FSVP.

The SEM images of the microstructures of FSV-processed samples are shown in Fig. 11. Two kinds of particles can be observed in the images: continuous particles (denoted by yellow arrows) and bright and seemingly distinct particles (denoted by red arrows). The EDS analysis results for the particles indicated by yellow arrows are also presented in Fig. 11. The Si peaks observed for these particles indicate that they are SiC particles. It can be seen that the agglomeration of reinforcing particles (shown by the yellow arrow) and the size of β particles (shown by the red arrow) decreased as the vibration frequency increased. It has been previously mentioned that the high vibration frequency increased the material deformation in the stir zone, and this resulted in a more homogeneous distribution of SiC particles. A decrease in the β-particles size by the increment of the vibration frequency may be related to the effect of the workpiece vibration in FSVP on heat generation. Barooni *et al*. [39] measured the temperature during FSVW and found an increase in heat generation and temperature as the welded specimens were vibrated. They noted that vibration improves the friction between the tool and the welded specimens. Based on the Mg–Al phase diagram, the dissolution temperature of the β phase or $Mg_{17}Al_{12}$ phase is around 437°C. Baradarani *et al*. [20] found that high temperatures during UaFSP led to the dissolution of β particles.

Table 1 summarizes the stir zone grain sizes and mechanical characteristics values of FS- and FSV-processed samples for different traverse speeds and vibration frequencies. It has been mentioned that increasing the traverse speed during FSP or the vibration frequency during FSVP resulted in grain refinement as well as a more homogeneous distribution of second-phase particles. Table 1 shows that the ultimate tensile strength (UTS) of FS processed specimen increases from 155.34 to 324.97 MPa as the transverse speed increases from 40 to 95 mm/min. Table 1 also indicates that UTS of FSV processed specimen increases from 292.57 to 361.82 MPa as the vibration frequency increases. These can be related to the roles of grain size and SiC particles distribution on strength. It was mentioned before that grain size decreased and particles distributed more homogenously as tool transverse speed increased (during FSP) and vibration frequency increased (during FSVP). By reduction of the grain size, the volume fraction of grain boundaries increases, and the mobility of dislocations reduces [28]. Based on the Hall–Petch equation ($\sigma = \sigma_0 + kd^{-\frac{1}{2}}$) [28] (where σ_0 is a material constant and k is the strengthening coefficient), strength (σ) enhances as grain size (d) reduces. Additionally, less agglomeration means uniformly distributed smaller particles with lower separating distance. For a volume fraction of particles (f), the free distance between the particles (λ) is obtained from the following relationship [39]:

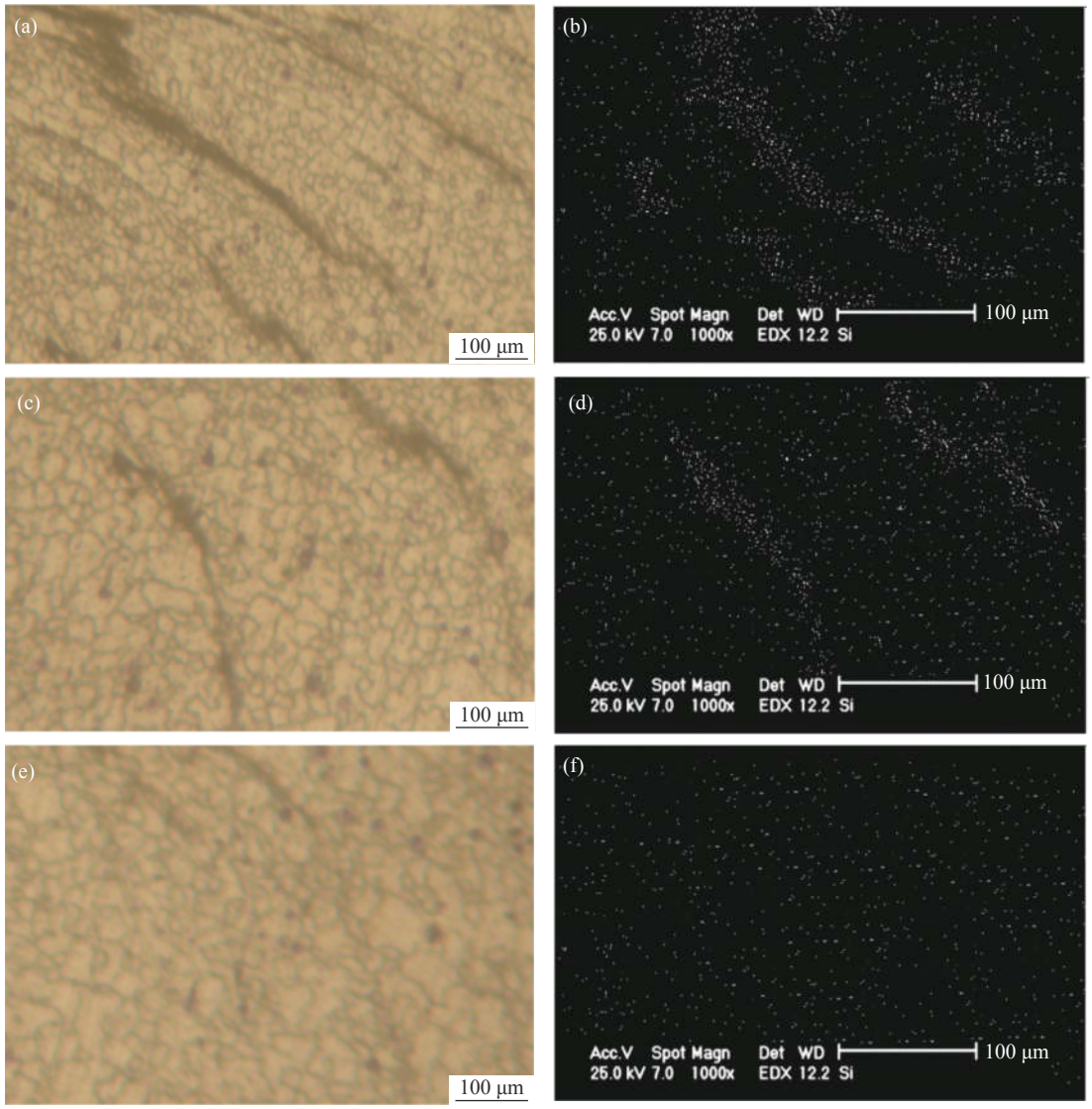

Fig. 10. (a, c, e) Microstructures and (b, d, f) EDX maps showing the distribution of Si element during FSVP under different vibration frequencies (rotational speed of 1250 r/min; traverse speed of 63 mm/min): (a, b) 20 Hz; (c, d) 35 Hz; (e, f) 50 Hz.

$$\lambda = \frac{4(1-f)r}{3f} \tag{4}$$

where λ decreases as r (particle size) decreases. Based on Orowan mechanism the strengthening effect ($\Delta\sigma$) of second-phase particles is dependent on particle size (r) and the distance of particles from each other (λ) [40]:

$$\Delta\sigma = \frac{0.13Gb}{\lambda} \ln\frac{r}{b} \tag{5}$$

where G and b are shear modulus and Burgers vector, respectively. According to Eq. (5), the influence of λ on strengthening is greater than the effect of r, and $\Delta\sigma$ increases as λ decreases. The grain size decrease and the increase of distribution homogeneity both increase the strength. Consequently, with an increase in the traverse speed, FS-processed samples feature increased strength, and with an increase in the vibration frequency, FSV-processed samples feature increased strength.

Table 1 also shows that with an increase in the traverse speed or vibration frequency, the elongation increases. The elongation for FS-processed specimen increases from 11.32% to 15.24% as the transverse speed increases from 40 to 95 mm/min, and the elongation for FSV-processed specimen increases from 12.26% to 16.88% as the vibration frequency increases from 20 to 50 Hz. This can also be associated with the decrease in the grain size and the improvement of the particle distribution. The volume fraction of grain boundaries develops, as grain size reduces, Grain boundaries reduce the crack growth and, as a result, increase the elongation [41]. On the other hand, large agglomerated particles are preferable sites for crack initiation. As agglomeration decreases and particles distribute more homogeneously, crack initiation is hindered, and as a result, the elongation increases.

Table 1 also compares the formability index of the invest-

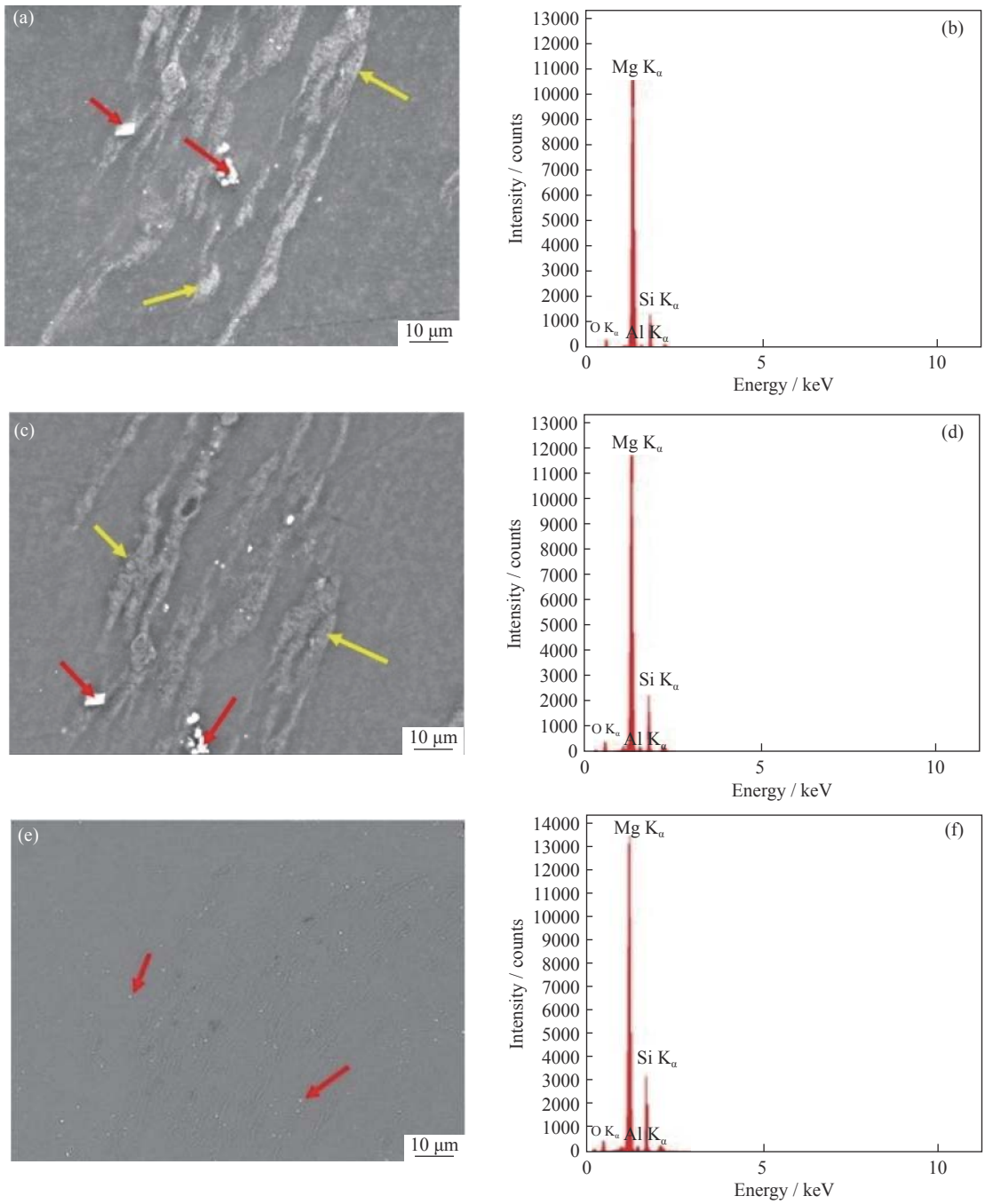

Fig. 11. (a, c, e) SEM images and (b, d, f) EDS analyses of particles results of FSV-processed samples subjected to different vibration frequencies: (a, b) 20 Hz; (c, d) 35 Hz; (e, f) 50 Hz. Red arrows indicate β-phase particles, and yellow arrows indicate reinforcing particles (rotational speed of 1250 r/min; traverse speed of 63 mm/min).

igated specimens. The formability index is a factor for evaluating toughness and is defined as the multiplication of ductility (E.L.) and strength (UTS): UTS × E.L. [42]. It is shown in Table 1 that the formability index of FS-processed samples increases from 1758.45 to 4952.54 MPa·% with the traverse speed increasing, and likewise, the formability index of FSV-processed specimens increases from 3586.91 to 6107.52 MPa·% with the vibration frequency increasing. This is related to the impact of vibration frequency and traverse speed on the strength and ductility of the processed samples. The strength and ductility were observed to improve as the traverse speed and vibration frequency increased.

Fig. 12 illustrates the distribution of hardness in the cross sections of the studied samples. It is evident that by increasing the traverse speed and vibration frequency, the hardness in different zones increased. The higher hardness can be attributed to the more grain refinement and the more homogeneous distribution of the strengthening particles as the traverse

Table 1. Grain sizes and mechanical characteristics of as-received, FS-processed and FSV-processed samples containing SiC particles (rotational speed of 1250 r/min)

Sample	Grain size / μm	UTS / MPa	Elongation / %	Formability index / (MPa·%)
As-received	140.00	124.56	10.10	1252.40
FSP, 40 mm/min	53.23 ± 2.00	155.34	11.32	1758.45
FSP, 63 mm/min	39.43 ± 2.00	283.67	12.83	3639.48
FSP, 95 mm/min	30.71 ± 2.00	324.97	15.24	4952.54
FSVP, 20 Hz, 40 mm/min	33.32 ± 2.00	292.57	12.26	3586.91
FSVP, 35 Hz, 63 mm/min	26.43 ± 2.00	335.61	13.54	4544.16
FSVP, 50 Hz, 95 mm/min	20.02 ± 2.00	361.82	16.88	6107.52

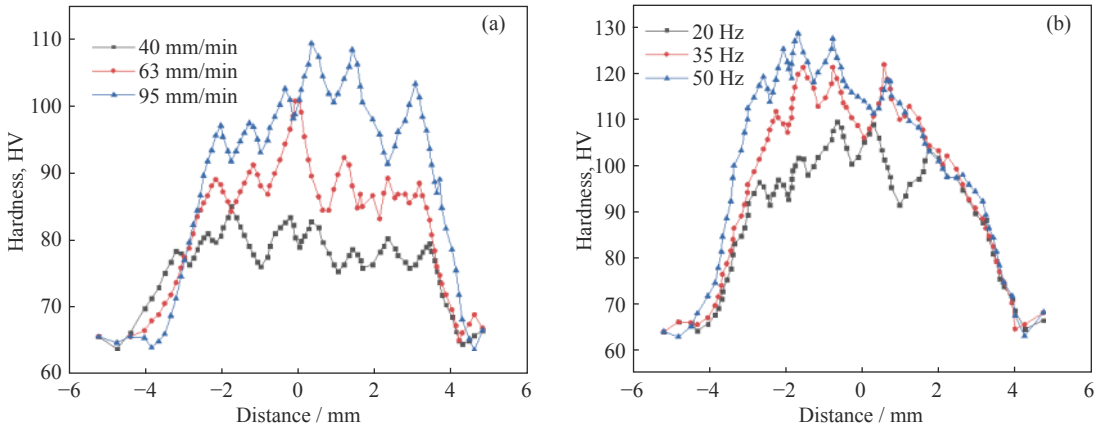

Fig. 12. Hardness of the specimens produced by (a) FSP and (b) FSVP. The rotational speed is 1250 r/min for both processes, and the traverse speed is 63 mm/min for FSVP.

speed and vibration frequency increased. Hardness is donated as the ability of a substance to withstand plastic deformation, and it has an inverse relationship with dislocation movement [43]. A reduction in grain size and an increase in the homogeneous distribution of particles both lead to a retardation in dislocation movement and an increase in hardness [44].

One noticeable characteristic of Mg alloys is their high strength-to-mass ratio. Fig. 13 presents the strength-to-mass ratios of an as-received specimen and processed ones. The ratio of the as-received specimen is the lowest, and those of the FS- and FSV-processed samples increase with an increase in traverse speed and vibration frequency, respectively. The higher strength-to-mass ratio of processed specimens compared with that of as-received specimens is not only associ-

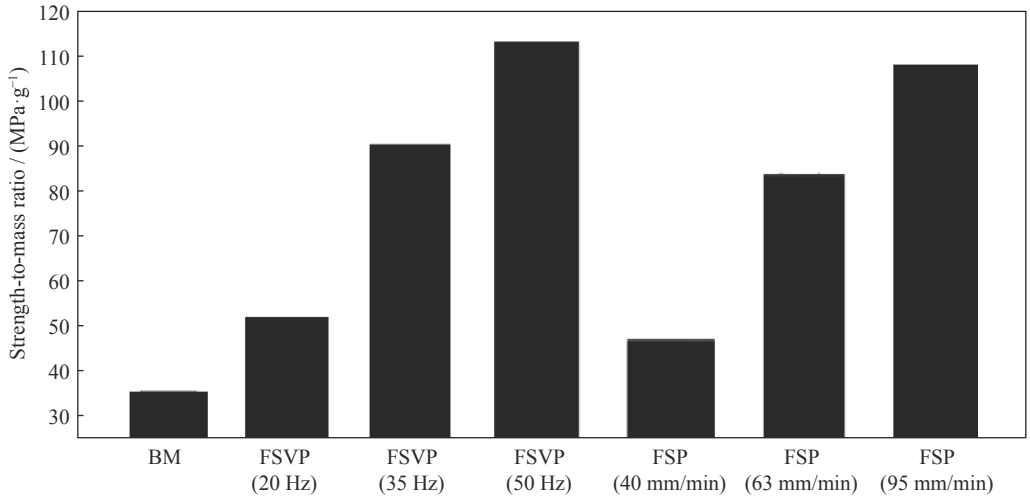

Fig. 13. Influence of FSP and FSVP on the strength-to-mass ratio for different processing conditions: vibration frequencies of 20, 35, and 50 Hz for FSV-processed specimens and traverse speeds of 40, 63, and 95 mm/min for FS-processed specimens.

ated with grain refinement and the presence of strengthening particles in the microstructure of the processed samples; it may also be related to the absence of defects in the microstructures of FS- and FSV-processed specimens. Previous findings have indicated that casting defects (such as shrinkage cavities and porosities) are omitted by the application of FSP and FSVP [45].

Fig. 14 shows the fracture surface images of studied samples for FSP and FSVP. The fracture surfaces are full of dimples. These dimples indicate that the fracture is ductile. Ductile fracture is initiated by the nucleation of voids. The voids grow and coalescence and eventually form cracks and result in fracture [46]. Voids normally nucleate on dislocation locks as well as around the second-phase particles present in the microstructure [46]. It has been found that the voids that initiate around the particles are larger than those that initiate on locks and they have more effect on fractures. Non-homogeneous distribution of reinforcing SiC particles and the presence of large agglomerated particles lead to the initiation of large voids. The parameters that enhance the homogeneity distribution of particles result in small-size voids, and this hinders the propagation of fractures.

Fig. 14 displays that the voids for the FS-processed samples are larger than those of the FSV-processed speci-

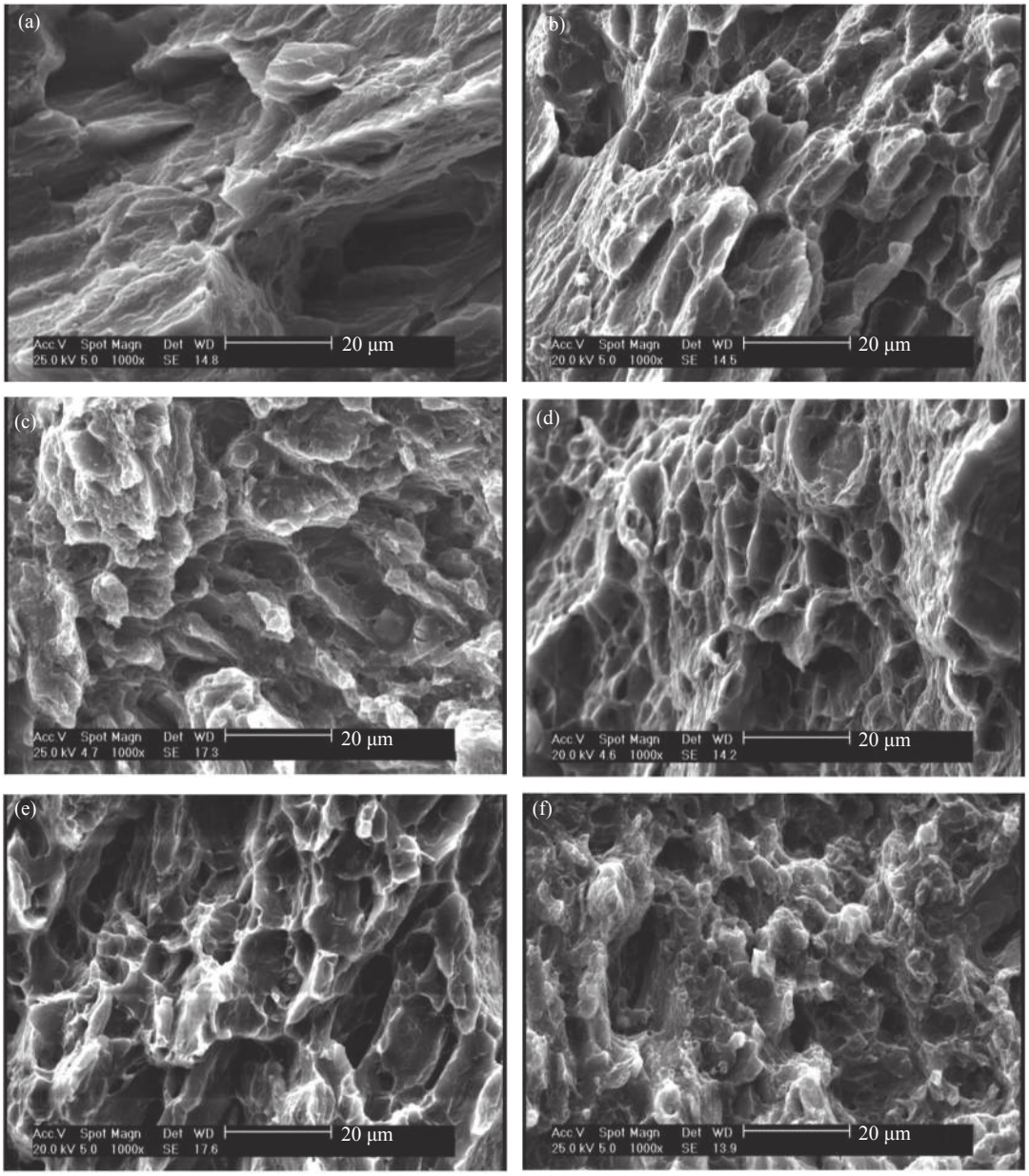

Fig. 14. Fracture surfaces of (a, c, e) FS-processed specimens and (b, d, f) FSV-processed specimens. The traverse speeds are (a–b) 40 mm/min, (c–d) 63 mm/min, and (e–f) 95 mm/min; the vibration frequencies are (b) 20 Hz, (d) 35 Hz, and (f) 50 Hz; the rotational speed is 1250 r/min.

mens. The figure also indicates that the void size for FS-processed specimens decreases as the traverse speed increases, and likewise, that for the FSV-processed samples decreases as the vibration frequency and the traverse speed increases. As mentioned previously, these can be related to the effect of particle distribution on void initiation.

4. Conclusion

In the current investigation, a modified version of FSP, called FSVP, was implemented to fabricate AZ91/SiC surface composites. The mechanical characteristics and microstructure of the composites developed by both methods, FSP and FSVP, were evaluated. The effects of the traverse speed of the tool as well as the vibration frequency of the workpiece on the microstructure and different characteristics of the developed composites were analyzed. The results displayed that the mechanical characteristics of the FSV-processed samples were higher than those of the FS-processed samples. Due to the workpiece vibration, the FSVP resulted in a higher material deformation than the FSP. This increased the DR and led to the development of finer grains. Additionally, the higher material deformation during FSVP led to a more homogeneous distribution of SiC particles. The results also indicate that with an increase in the vibration frequency and the traverse speed of the welding tool, the stir zone grain size of the FSV-processed samples reduced and the particle distribution homogeneity improved. The FSVP is therefore suggested as an "easy-to-apply" method for various industries compared with the FSP.

Acknowledgements

The authors would like to thank the Amirkabir University of Technology (AUT), Sharif University of Technology, and the National Elites Foundation of Iran for their support during this research.

References

[1] M. Abbasi, A. Abdollahzadeh, B. Bagheri, and H. Omidvar, The effect of SiC particle addition during FSW on microstructure and mechanical properties of AZ31 magnesium alloy, *Int. J. Mater. Eng. Perform.*, 24(2015), No. 12, p. 5037.

[2] A. Abdollahzadeh, A. Shokuhfar, H. Omidvar, J.M. Cabrera, A. Solonin, A. Ostovari, and M. Abbasi, Structural evaluation and mechanical properties of AZ31/SiC nano-composite produced by friction stir welding process at various welding speeds, *Proc. Inst. Mech. Eng. Part L J. Mater. Des. Appl.*, 233(2019), No. 5, p. 831.

[3] B.L. Mordike and T. Ebert T, Magnesium properties applications potential, *Mater. Sci. Eng. A*, 302(2001), p. 37.

[4] J. Goken, J. Bohlen, N. Hort, D. Letzig, and K.U. Kainer, New development in magnesium technology for light weight structures in transportation industries, *Mater. Sci. Forum*, 426-432(2003), p. 153.

[5] A. Abdollahzadeh, A. Shokuhfar, J.M. Cabrera, A.P. Zhilyaev, and H. Omidvar, *In-situ* nanocomposite in friction stir welding of 6061-T6 aluminum alloy to AZ31 magnesium alloy, *J. Mater. Process. Technol.*, 263(2019), p. 296.

[6] A. Abdollahzadeh, A. Shokuhfar, J.M. Cabrera, A.P Zhilyaev, and H. Omidvar, The effect of changing chemical composition on dissimilar Mg/Al friction stir welded butt joints using zinc interlayer, *J. Manuf. Processes*, 34(2018), p. 18.

[7] B.B. Straumal, X. Sauvage, B. Baretzky, A.A. Mazilkin, and R.Z. Valiev, Grain boundary films in Al–Zn alloys after high pressure torsion, *Scripta Mater.*, 70(2014), p. 59.

[8] A. Galiyev, R. Kaibyshev, and G. Gottstein, Correlation of plastic deformation and dynamic recrystallization in magnesium alloy ZK60, *Acta. Mater.*, 49(2001), No. 7, p. 1199.

[9] M.T. Pérez-Prado, J.A. del Valle, and O.A. Ruano, Grain refinement of Mg−Al−Zn alloys via accumulative roll bonding, *Scripta Mater.*, 51(2004), No. 11, p. 1093.

[10] M. Abbasi, A. Abdollahzadeh, H. Omidvar, B. Bagheri, and M. Rezaei, Incorporation of SiC particles in FS Welded zone of AZ31 Mg alloy to improve the mechanical properties and corrosion resistance, *Int. J. Mater. Res.*, 107(2016), No. 6, p. 566.

[11] P. Asadi, M.K. Besharati Givi, and G. Faraji, Producing ultrafine-grained AZ91 from as-cast AZ91 by FSP, *Mater. Manuf. Processes*, 25(2010), No. 11, p. 1219.

[12] H.S. Arora, H. Singh, B.K. Dhindaw, and H.S. Grewal, Some investigations on friction stir processed zone of AZ91 alloy, *Trans. Indian Inst. Met.*, 65(2012), No. 6, p. 735.

[13] D. Ahmadkhaniha, M. Heydarzadeh Sohi, A. Salehi, and R. Tahavvori, Formations of AZ91/Al_2O_3 nano-composite layer by friction stir processing, *J. Magnes. Alloys*, 4(2016), No. 4, p. 314.

[14] A.H. Feng, B.L. Xiao, Z.Y. Ma, and R.S. Chen, Effect of friction stir processing procedures on microstructure and mechanical properties of Mg–A–Zn casting, *Metall. Mater. Trans. A*, 40(2009), No. 10, p. 2447.

[15] P. Asadi, M.K. Besharati Givi, K. Abrinia, M. Taherishargh, and R. Salekrostam, Effects of SiC particle size and process parameters on the microstructure and hardness of AZ91/SiC composite layer fabricated by FSP, *J. Mater. Eng. Perform.*, 20(2011), No. 9, p. 1554.

[16] M. Abbasi, B. Bagheri, M. Dadaei, H. Omidvar, and M. Rezaei, The effect of FSP on mechanical, tribological, and corrosion behavior of composite layer developed on magnesium AZ91 alloy surface, *Int. J. Adv. Manuf. Technol.*, 77(2015), No. 9-12, p. 2051.

[17] M. Dadaei, H. Omidvar, B. Bagheri, M. Jahazi, and M. Abbasi, The effect of SiC/Al_2O_3 particles used during FSP on mechanical properties of AZ91 magnesium alloy, *Int. J. Mater. Res.*, 105(2014), No. 4, p. 369.

[18] H.R. Eftekharnia, A.A. Amadeh, A. Khodabandeh, and M. Paidar, Microstructure and wear behavior of AA6061/SiC surface composite fabricated via friction stir processing with different pins and passes, *Rare Met.*, 39(2020), p. 429.

[19] S.K. Kumar, Ultrasonic assisted friction stir processing of 6063 aluminum alloy, *Arch. Civil Mech. Eng.*, 16(2016), No. 3, p. 473.

[20] F. Baradarani, A. Mostafapour, and M. Shalvandi, Enhanced corrosion behavior and mechanical properties of AZ91 magnesium alloy developed by ultrasonic-assisted friction stir processing, *Mater. Corros.*, 71(2020), No. 1, p. 109.

[21] R. Farshbaf Zinati, Development of a modified friction stir process for dispersion of multi-walled carbon nano-tube throughout

nylon 6, *Mod. Mech. Eng.*, 15(2015), No. 5, p. 269.
[22] B. Bagheri and M. Abbasi, Development of AZ91/SiC surface composite by FSP: Effect of vibration and process parameters on microstructure and mechanical characteristics, *Adv. Manuf.*, 8(2020), No. 1, p. 82.
[23] ASTM International, ASTM-E112-13: *Standard Test Methods for Determining Average Grain Size*, West Conshohocken, 2010.
[24] ASTM International, ASTM-E8M: *Standard Test Methods of Tension Testing of Metallic Materials*, American Soc. Test. Mater., West Conshohocken, Pennsylvania, 2003.
[25] M. Abbasi, B. Bagheri, and R. Keivani, Thermal analysis of friction stir welding process and investigation into affective parameters using simulation, *J. Mech. Sci. Technol.*, 29(2015), No. 2, p. 861.
[26] M. Paidar, O.O. Ojo, H.R. Ezatpour, and A. Heidarzadeh, Influence of multi-pass FSP on the microstructure, mechanical properties and tribological characterization of Al/B_4C composite fabricated by accumulative roll bonding (ARB), *Surf. Coat. Technol.*, 361(2019), p. 159.
[27] B. Bagheri, M. Abbasi, A. Abdollahzadeh, and H. Omidvar, Advanced approach to modify friction stir spot welding process, *Met. Mater. Int.* (2019). https://doi.org/10.1007/s12540-019-00416-x
[28] D. Hull and D.J. Bacon, *Introduction to Dislocations*, 5th ed., Butterworth-Heinemann, Britain, 2011.
[29] T.R. McNelley, S. Swaminathan, and J.Q. Su, Recrystallization mechanisms during friction stir welding/processing of aluminum alloys, *Scripta Mater.*, 58(2008), No. 5, p. 349.
[30] M. Abbasi, M. Givi, and B. Bagheri, Application of vibration to enhance efficiency of friction stir processing, *Trans. Nonferrous Met. Soc. China*, 29(2019), No. 7, p. 1393.
[31] C.I. Chang, C.J. Lee, and J.C. Huang, Relationship between grain size and Zener–Holloman parameter during friction stir processing in AZ31 Mg alloys, *Scripta Mater.*, 51(2004), No. 6, p. 509.
[32] W.D. Callister and D.G. Rethwisch, *Materials Science and Engineering: An Introduction*, Wiley, Utah, 2007.
[33] Y.S. Li, Y. Zhang, N.R. Tao, and K. Lu, Effect of the Zener-Hollomon parameter on the microstructures and mechanical properties of Cu subjected to plastic deformation, *Acta Mater.*, 57(2009), No. 3, p. 761.
[34] M. Abbasi, M. Givi, and A. Ramazani, Friction stir vibration processing: A new method to improve the microstructure and mechanical properties of Al5052/SiC surface nano-composite layer, *Int. J. Adv. Manuf. Technol.*, 100(2019), No. 5-8, p. 1463.
[35] D.A. Porter, K.E. Easterling, and M.Y. Sherif, *Phase Transformation in Metals and Alloys*, 3rd ed., CRC Press, New York, 2009, p. 156.
[36] G.E. Dieter, *Mechanical Metallurgy*, McGraw-Hill Book Company, New York, 1988.
[37] M. Maghsoodi and Z. Yari, Effect of temperature on wet agglomeration of crystals, *Iran J. Basic Med. Sci.*, 17(2014), No. 5, p. 344.
[38] M.N. Gajanan, S. Narendranath, and S.S. Satheesh Kumar, Effect of grain refinement on mechanical and corrosion behavior of AZ91 magnesium alloy processed by ECAE, *IOP Conf. Ser. Mater. Sci. Eng.*, 591(2019), No. 1, p. 19.
[39] O. Barooni, M. Abbasi, M. Givi, and B. Bagheri, New method to improve the microstructure and mechanical properties of joint obtained using FSW, *Int. J. Adv. Manuf. Technol.*, 93(2017), No. 9, p. 4371.
[40] Z.Y. Ma, A.L. Pilchak, M.C. Juhas, and J.C. Williams, Microstructural refinement and property enhancement of cast light alloys via friction stir processing, *Scripta Mater.*, 58(2008), No. 5, p. 361.
[41] V. Uthaisangsuk, *Microstructure Based Formability Modeling of Multiphase Steels* [Dissertation], IEHK, RWTH-Aachen, 2009.
[42] M. Naderi, M. Abbasi, and A. Saeed-Akbari, Enhanced mechanical properties of a hot-stamped advanced high-strength steel via tempering treatment, *Metall. Mater. Trans. A*, 44(2013), No. 4, p. 1852.
[43] M. Paidar, A. Asgari, O.O. Ojo, and A. Saberi, Mechanical properties and wear behavior of AA5182/WC nanocomposite fabricated by friction stir welding at different tool traverse speeds, *J. Mater. Eng. Perform.*, 27(2018), No. 4, p. 1714.
[44] A. Moghanian, M. Paidar, S.S. Seyedafghahi, and O.O. Ojo, Friction stir welding of pure magnesium and polypropylene in a lap-joint configuration: Microstructure and mechanical properties, *Int. J. Miner. Metall. Mater.*, 26(2019), No. 6, p. 766.
[45] Q. Yang, B.L. Xiao, and Z.Y. Ma, Influence of process parameters on microstructure and mechanical properties of friction-stir-processed Mg−Gd−Y−Zr casting, *Metall. Mater. Trans. A*, 43(2012), No. 6, p. 2094.
[46] B. Bagheri, M. Abbasi, and R. Hamzeloo, The investigation into vibration effect on microstructure and mechanical characteristics of friction stir spot vibration welded aluminum: Simulation and experiment, *Proc. Inst. Mech. Eng. Part C J. Mech. Eng. Sci.*, 234(2020), No. 9, p. 1809.